Modeling and experimental validation of field distributions due to eddy currents in slitted conducting plates

Please check the document version of this publication:

• A submitted manuscript is the version of the article upon submission and before peer-review. There can be important differences between the submitted version and the official published version of record. People interested in the research are advised to contact the author for the final version of the publication, or visit the DOI to the publisher's website.
• The final author version and the galley proof are versions of the publication after peer review.
• The final published version features the final layout of the paper including the volume, issue and page numbers.

Link to publication

Modeling and Experimental Validation of Field Distributions due to Eddy Currents in Slitted Conducting Plates

C.H.H.M. Custers [1], J.W. Jansen [1] and E.A. Lomonova [1]

[1]Electromechanics and Power Electronics, Eindhoven University of Technology, 5600 MB Eindhoven, The Netherlands

Email:c.h.h.m.custers@tue.nl

Abstract—The paper describes a 3D semi-analytical harmonic modeling technique, which is capable to model eddy current distributions in conducting structures and the associated fields. The induced current density and magnetic fields in the spectral domain are described, where a spatially varying conductivity of a conducting region is incorporated in the solutions of magnetic-field quantities. An experimental setup is used to measure the field distribution above differently shaped conducting plates, placed on top of a coil, in which eddy currents are induced. The measurement results are compared to simulation results and the perturbations are analyzed.

Index Terms—Analytical Modeling, Eddy current, Fourier analysis, Permanent Magnet Machines, Experimental Validation.

I. INTRODUCTION

In synchronous permanent magnet devices, eddy currents are induced in conducting parts, such as magnets and cooling plates, due to movement and ac magnetic fields. In nano-meter accurate positioning devices, used in e.g. the semi-conductor manufacturing industry, such as planar motors [1], [2] and core-less linear motors [3], the parasitic force due to the eddy currents can reduce the performance [4], [5]. Analysis of the transient eddy current distribution can give important information on the spatial and time dependent harmonic content, which can be used to increase the performance of the machines.

To calculate these eddy currents and parasitics created by them, the finite element method (FEM) is an often used method. To accurately model eddy current effects for motors such as the linear and planar motor mentioned before, the geometrical shape of the conducting material has to be taken into account in all three dimensions. However, the large open boundary structures of these type of motors makes the 3D FEM have a relatively high computational load. For this reason, a semi-analytical harmonic (Fourier solutions based) method has been researched as an alternative for the FE method. The developed harmonic model is capable, in contrast to classical harmonic models, of calculating eddy currents in complex segmented conducting structures. The method is an extension of a 2D model described in [6], taking also segmentation in the third dimension into account. The model has shown good agreement with FEM.

In this paper, a semi-analytical method to model eddy currents in slitted conducting plates is presented. This method
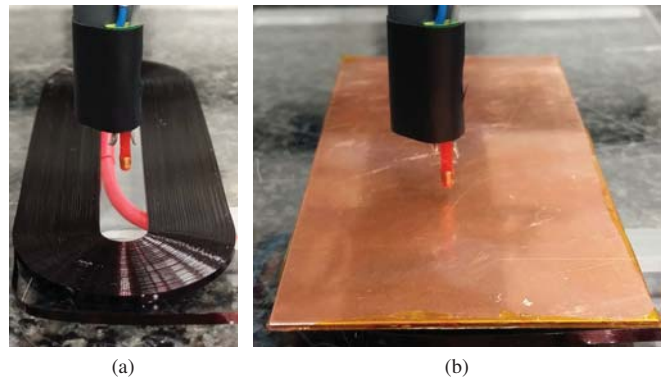

Fig. 1. The used measurement setup. a) Source coil (race-track shaped) with above it a very small pick-up coil, wound around a red non-magnetic core. b) A copper plate is placed on top of the coil and the pick-up coil is located above.

can be used to analyze eddy currents in the cooling system of a moving-magnet planar motor. As this paper focuses on the validation of the semi-analytical method using measurements, a electromagnetic configuration is used that only consists of a single coil and a copper plate. By using a copper plate, the eddy current density will be high, allowing good visualization of the eddy currents effect using measurements. In a normal cooling system, materials with a lower conductivity would be used to minimize the eddy current effect. However, in nano-meter accurate positioning systems, the parasitic effects due to eddy currents impair the performance. The used experimental set-up will be described first. Then the (Fourier based) model formulation will be discussed for conducting regions. To verify the developed model it will be compared to measurements and the results will be analyzed.

II. EXPERIMENTAL SETUP

The experimental setup used for validation of the semi-analytical model is shown in Fig. 1. A race-track shaped coil made of fine rectangular copper wire is placed in air. Above the coil a copper plate is placed. A 50 μm thick airgap is present between the coils and the plate. The time varying current in the coils will produce an ac magnetic field and this will induce (eddy) currents in the copper plate. Several plates will be placed above the coil, a solid plate and two
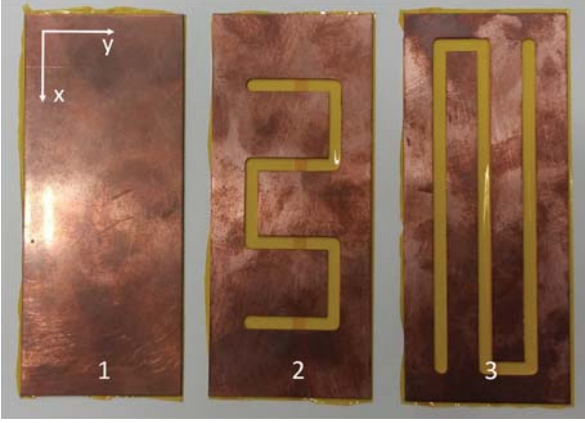
Fig. 2. The three copper plates that were used for the measurement. The bottom side of the plates is covered with polyimide film for isolation purposes.

plates with a certain slit pattern, where the slits will change the spatial distribution of the magnetic field. These kind of slits are often used in cooling systems, to reduce the eddy currents. The three plates are shown in Fig. 2, where they are numbered for the remainder of the paper. The copper plates are placed directly on top of the coil, therefore, the bottom side of the plates is covered with a polyimide film for isolation.

As a harmonic (Fourier based) modeling technique is utilized to calculate the magnetic fields, the geometric model of the electromagnetic configuration of Fig. 1 is assumed to be periodical in both the x- and y-directions. However, as the measurement set-up will on consist of a single 'period', and is not repeating in the x- or y-direction, air is added on both sides of the periodical section. The periodic width in both directions is almost double of the coil width in that direction. In this way, the influence of the magnetic fields of adjacent periods is minimized. In the z-direction, the model is divided into regions. The source coil is located in Region 2, where Region 1, 3 and 5 are regions containing only air. The (Fourier based) formulation of the magnetic fields in these regions, are described in [7]. In the conducting region (Region 4), where the copper plate is located, the conductivity will vary as a function of position, hence outside the plate and inside the slits (where air is present) the conductivity is zero.

III. HARMONIC MODEL FORMULATION IN CONDUCTING REGIONS

The magnetic field solutions are based on the quasi-static Maxwell's equations. This means the displacement current, $\frac{\partial \vec{D}}{\partial t}$, is neglected. The time derivative is denoted by $j\omega$. Maxwell's equations are then given by

$$\nabla \times \vec{E} = -j\omega \vec{B}, \tag{1}$$
$$\nabla \times \vec{H} = \vec{J}, \tag{2}$$
$$\nabla \cdot \vec{B} = 0, \tag{3}$$
$$\nabla \cdot \vec{J} = 0 \text{ (no free charge)}, \tag{4}$$

where $\vec{E}$ is the electric field intensity, $\vec{B}$ the magnetic flux density, $\vec{H}$ the magnetic field strength, $\vec{J}$ is current density and ρ is the electric charge density. The relation between the magnetic flux density and the magnetic field strength is given by the constitutive relation

$$\vec{B} = \mu_0 \mu_r \vec{H}, \tag{5}$$

where μ_0 is the permeability of vacuum and μ_r is the relative permeability, which is equal to 1 throughout the model. The eddy current density $\vec{J}^{eddy}$ is obtained from the electric field

$$\vec{J}^{eddy} = \sigma(x,y)\vec{E}. \tag{6}$$

After substitution of (5) and (6) into (1) and (2), equations (1) and (2) are written separately for each Cartesian component of $\vec{E}$ and $\vec{H}$. The expressions for the z-components are substituted in the remaining equations, resulting in

$$\partial_z E_x = j\omega\mu_0 H_y - \partial_x \left(\sigma(x,y)^{-1} \left(\partial_x H_y - \partial_y H_x \right) \right), \tag{7}$$
$$\partial_z E_y = -j\omega\mu_0 H_x - \partial_y \left(\sigma(x,y)^{-1} \left(\partial_x H_y - \partial_y H_x \right) \right), \tag{8}$$
$$\partial_z H_x = -\sigma(x,y) E_y + (j\omega\mu_0)^{-1} \partial_x \left((\partial_x E_y - \partial_y E_x) \right), \tag{9}$$
$$\partial_z H_y = \sigma(x,y) E_x + (j\omega\mu_0)^{-1} \partial_y \left((\partial_x E_y - \partial_y E_x) \right). \tag{10}$$

To find a solution to these four equations, the method of separation of variables is applied. As mentioned before, a harmonic basis for the solution in the x- and y-directions is chosen. This means that every quantity, that is a function of x and y, is written as a double truncated Fourier series

$$f(x,y) = \sum_{m=-M/2}^{M/2} \sum_{n=-N/2}^{N/2} \mathbf{f}_{n,m} \, e^{j(k_{x,n}x + k_{y,m}y)}, \tag{11}$$

where the spatial frequencies $k_{x,n}$ and $k_{y,m}$, are given by

$$k_{x,n} = \frac{n\pi}{\tau_x}, \tag{12}$$
$$k_{y,m} = \frac{m\pi}{\tau_y}, \tag{13}$$

where τ_x is half of the periodic width in the x-direction and τ_y is half of the periodic width in the y-direction. To model the electromagnetic configuration used for verification (Fig. 1), τ_x and τ_y are set to 80 mm and 50 mm respectively. The coefficients of the double Fourier sum per harmonic pair n, m are collected in a column vector denoted by $\mathbf{f}$. The Fourier series is truncated for implementation purposes and the number of harmonics used in the x- and y-direction is equal to $N + 1$ and $M + 1$ respectively.

To obtain the solution in the z-direction, (7)-(10) are written in two matrix equations in the spectral domain,

$$\frac{\partial}{\partial z} \begin{bmatrix} \mathbf{e_x} \\ \mathbf{e_y} \end{bmatrix} = \mathbf{F} \begin{bmatrix} \mathbf{h_x} \\ \mathbf{h_y} \end{bmatrix}, \tag{14}$$
$$\frac{\partial}{\partial z} \begin{bmatrix} \mathbf{h_x} \\ \mathbf{h_y} \end{bmatrix} = \mathbf{G} \begin{bmatrix} \mathbf{e_x} \\ \mathbf{e_y} \end{bmatrix}, \tag{15}$$
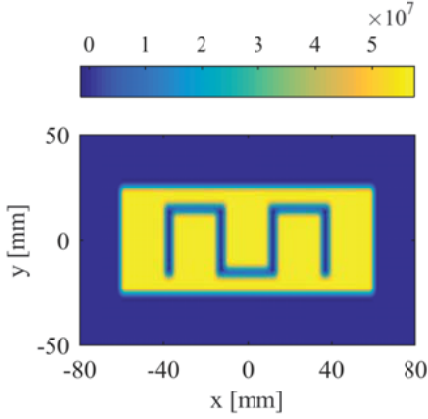
Fig. 3. Fourier representation of the conductivity in the conducting region, for N=120 and M=42.

where,

$$F = \begin{bmatrix} -\mathbf{K_x}\boldsymbol{\mathcal{P}}^{-1}\mathbf{K_y} & j\omega\mu_0\mathbf{I} + \mathbf{K_x}\boldsymbol{\mathcal{P}}^{-1}\mathbf{K_x} \\ -j\omega\mu_0\mathbf{I} - \mathbf{K_y}\boldsymbol{\mathcal{P}}^{-1}\mathbf{K_y} & \mathbf{K_y}\boldsymbol{\mathcal{P}}^{-1}\mathbf{K_x} \end{bmatrix}, \tag{16}$$

and

$$G = \begin{bmatrix} (j\omega\mu_0)^{-1}\mathbf{K_x}\mathbf{K_y} & -\boldsymbol{\mathcal{P}} - (j\omega\mu_0)^{-1}\mathbf{K_x}^2 \\ \boldsymbol{\mathcal{P}} + (j\omega\mu_0)^{-1}\mathbf{K_y}^2 & -(j\omega\mu_0)^{-1}\mathbf{K_y}\mathbf{K_x} \end{bmatrix}, \tag{17}$$

and $\mathbf{e_x}$, $\mathbf{e_y}$, $\mathbf{h_x}$ and $\mathbf{h_y}$ are the vectors containing the Fourier coefficients of E_x, E_y, H_x and H_y respectively and $\mathbf{I}$ is the identity matrix. The matrices $\mathbf{K_x}$ and $\mathbf{K_y}$ represent the derivatives to x and y respectively and contain the spatial frequencies $k_{x,n}$ and $k_{y,m}$ on the diagonal respectively. The matrix $\boldsymbol{\mathcal{P}}$ contains the information of the spatial dependency of the conductivity. The position dependent conductivity, that was introduced in (6), is described by a double Fourier series and its coefficients are arranged in the block-Toeplitz matrix $\boldsymbol{\mathcal{P}}$. By this arrangement, multiplication of a vector with the block-Toeplitz matrix, results in a 2D convolution of the coefficients and thus a multiplication of the series in the spatial domain. The incorporation of the spatially dependent conductivity causes thereby a coupling of the harmonics. The Fourier representation of the conductivity in the conducting region, when plate 2 is present (Fig. 2) is shown in Fig. 3. It crucial that sufficient harmonics are used to describe the conductivity distribution. If too few harmonics are used, the conductivity in the slits will not be equal to zero, which results in a less accurate result of the field computation. Especially for very thin slits, this means the number of harmonics that has to be used is relatively high.

Substituting (14) into (15) it is obtained that

$$\frac{\partial^2}{\partial z^2} \begin{bmatrix} \mathbf{h_x} \\ \mathbf{h_y} \end{bmatrix} = \mathbf{GF} \begin{bmatrix} \mathbf{h_x} \\ \mathbf{h_y} \end{bmatrix}. \tag{18}$$

An eigenvalue decomposition is performed on the result of the matrix multiplication $\mathbf{GF}$, to propagation information for the region with varying conductivity

$$\begin{bmatrix} \mathbf{Q_x} \\ \mathbf{Q_y} \end{bmatrix} \boldsymbol{\Lambda}^2 \begin{bmatrix} \mathbf{Q_x} \\ \mathbf{Q_y} \end{bmatrix}^{-1} = \mathbf{GF}, \tag{19}$$

where $\boldsymbol{\Lambda}$ is a diagonal matrix containing the vector $\boldsymbol{\lambda}$ with propagation constants on the diagonal and $\mathbf{Q_x}$ and $\mathbf{Q_y}$ are matrices containing the eigenvectors belonging to each eigenvalue. Because in (18) a double derivative to z is performed, the matrix $\boldsymbol{\Lambda}$ is squared in (19). Using the obtained propagation information, the z-dependent solution can be constructed. The solution consists, as is standard in the Fourier based model for a Cartesian coordinate system, of an upward traveling and downward traveling wave. The Fourier coefficients of the magnetic field strength components $\mathbf{h_x}$, $\mathbf{h_y}$ and $\mathbf{h_z}$ are then equal to

$$\mathbf{h_x} = \mathbf{Q_x} \left(\mathbf{E}^+(\boldsymbol{\lambda}, z) \, \mathbf{c}^+ - \mathbf{E}^-(\boldsymbol{\lambda}, z) \, \mathbf{c}^- \right), \tag{20}$$

$$\mathbf{h_y} = \mathbf{Q_y} \left(\mathbf{E}^+(\boldsymbol{\lambda}, z) \, \mathbf{c}^+ - \mathbf{E}^-(\boldsymbol{\lambda}, z) \, \mathbf{c}^- \right), \tag{21}$$

$$\mathbf{h_z} = -j \left(\mathbf{K_x}\mathbf{Q_x} + \mathbf{K_y}\mathbf{Q_y} \right) \boldsymbol{\Lambda}^{-1} \\ \left(\mathbf{E}^+(\boldsymbol{\lambda}, z) \, \mathbf{c}^+ + \mathbf{E}^-(\boldsymbol{\lambda}, z) \, \mathbf{c}^- \right). \tag{22}$$

The vectors $\mathbf{c}^+$ and $\mathbf{c}^-$ contain unknowns per harmonic pair, which will be determined later. The coefficients of the magnetic flux density components can be obtained by using (5). The solution for the induced current density components, $\mathbf{j_x^{ind}}$, $\mathbf{j_y^{ind}}$ and $\mathbf{j_z^{ind}}$ are determined using (1) and (6)

$$\mathbf{j_x^{ind}} = \mathbf{Q_y} \, \boldsymbol{\Lambda} \left(\mathbf{E}^+(\boldsymbol{\lambda}, z) \, \mathbf{c}^+ + \mathbf{E}^-(\boldsymbol{\lambda}, z) \, \mathbf{c}^- \right) - j\mathbf{K_y}\mathbf{h_z}, \tag{23}$$

$$\mathbf{j_y^{ind}} = -\mathbf{Q_x} \, \boldsymbol{\Lambda} \left(\mathbf{E}^+(\boldsymbol{\lambda}, z) \, \mathbf{c}^+ + \mathbf{E}^-(\boldsymbol{\lambda}, z) \, \mathbf{c}^- \right) + j\mathbf{K_x}\mathbf{h_z}, \tag{24}$$

$$\mathbf{j_z^{ind}} = j\mathbf{K_y}\mathbf{h_x} - j\mathbf{K_x}\mathbf{h_y}. \tag{25}$$

The expressions for the magnetic field components in the non-conducting regions (Regions 1, 2, 3 and 5) are described in [7]. In Region 2, where the coil is present, a Fourier description of the current density distribution of the coil is needed as a source term. Instead of describing the geometry of the coil (and hence the current density distribution), the field of the coil, without any conducting plate on top, is measured. From this measurement, a backward transformation is performed to obtain the source terms of Region 2. In this way, coil imperfections are already incorporated in the source terms which excludes this as a source of error between measurement and simulation. To obtain the unknowns of each region, boundary conditions are applied between the regions as also explained in [7]. This will form a system of linear equations which can be solved to determine all unknowns.

IV. EXPERIMENTAL VERIFICATION

The properties of the coil producing the field, shown in Fig. 1 are given in Table I. The current through the source coil has a rms value of 3.2 A and the frequency is equal to 2 kHz. The pick-up coil, which is measuring the field, is attached to an H-bridge to accurately place it above the source coil. It has been made sure that the H-bridge does not influence
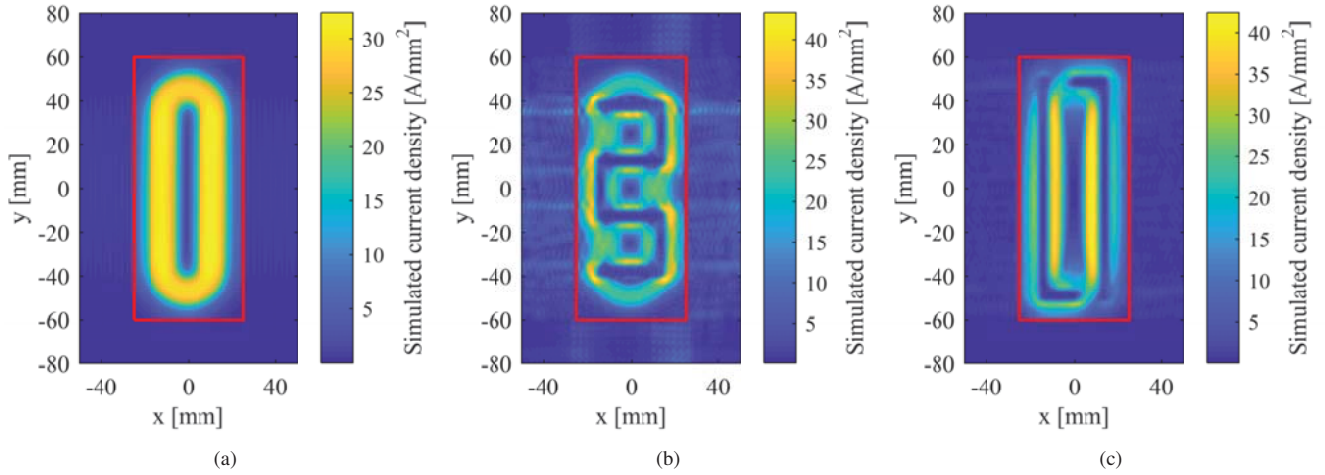
Fig. 4. Simulated current density in the conducting region (Region 4). The red square indicates the position of the plate. a) Plate 1. b) Plate 2. c) Plate 3.

TABLE I
PROPERTIES OF THE SOURCE COIL

Description	Value	Unit
Coil length (in x direction)	107.8	mm
Coil width (in y direction)	37.0	mm
Coil height	1.7	mm
Bundle width	14.3	mm
Number of turns	59.5	-

TABLE II
PROPERTIES OF THE CONDUCTING PLATES

Description	Value	Unit
Plate length (in x direction)	120.0	mm
Plate width (in y direction)	50.0	mm
Plate thickness	1	mm
Slit width	4	mm
Conductivity (copper @ 30° C)	5.73e7	S/m

the measurement, and no additional conducting materials are present near the setup. The properties of the conducting plates, that are placed on top of the source coil, are given in Table II. The pick-up coil is made of 30 μm thin copper wire, wound around a non-magnetic core with a diameter of 1.7 mm. The field is measured at 1 mm above the plates on a grid of 120 mm x 64 mm with a resolution of 1 mm. The z-component of the magnetic flux density is calculated from the measured voltage, V_{meas}, using

$$B_{z,meas} = \frac{V_{meas}}{T_{mc} \, A_{mc} \, \omega}, \tag{26}$$

where A_{mc} is the surface of the measurement coil (2.3 mm^2) and T_{mc} the number of turns of the measurement coil, which is equal to 103 and ω the radial frequency of the induced voltage.

All simulation results are calculated for $N = 120$ and $M = 42$. It has been verified that the conductivity description reaches zero inside the slits, with this number of harmonics. However, more harmonics can, because of computational

memory, not be used. The simulated induced current densities in the several plates is depicted in Fig. 4. It can be seen that the conductivity is correctly incorporated and that no current is flowing on the locations of the slits. Furthermore it is clear that the slits reduce the overall current density, however, the peak current is increased.

The measured magnetic flux densities with the different plates placed on top of the coil are shown in Fig. 5. The magnetic flux densities obtained with the developed modeling technique are depicted in Fig. 6. The absolute difference between the model and the measurement is shown in Fig. 7. A relative error is calculated through

$$\frac{\text{rms}(B_{z,meas} - B_{z,sim})}{\max{(B_{z,meas})}}. \tag{27}$$

It can be seen in Fig. 7a, that for plate 1 the model and measurement are in good agreement. The relative error is equal to 3 %. For plate 2 and 3 the error is larger, 11 % and 12 % respectively. As there are no slit patterns in plate 1, the used number of harmonics is relatively high. The error is therefore expected to originate from perturbations between measurement setup and model. Hence, the conductivity varies with temperature, and all measured quantities, such as the distance between the measurement coil and the plate, have tolerances. Furthermore, 2D finite element simulations of a rectangular wire coil with 10 turns, show a distribution of the current density with 10 % difference between the minimum and maximum value inside the coil, when a plate is positioned above. As the source terms of the Fourier model assume an uniformly distributed current density throughout the coil, a mismatch is caused. For plate 2, the error is highest at the location of the slits. As the absolute difference is larger on the right side of the plate than on the left side, the plate could have been of center during the measurement, which causes a discrepancy between the modeled and measured result. The relative error of plate 2 and plate 3 are furthermore due to the truncation of the harmonics in both directions. Increasing the
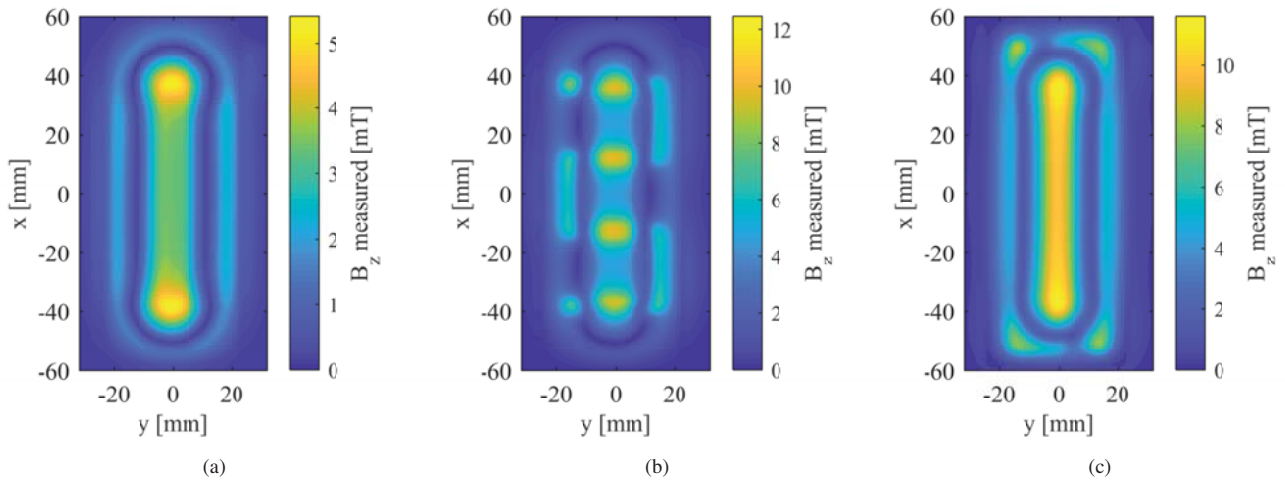
Fig. 5. Measured magnetic flux density in the z-direction with the experimental setup. a) Plate 1. b) Plate 2. c) Plate 3.
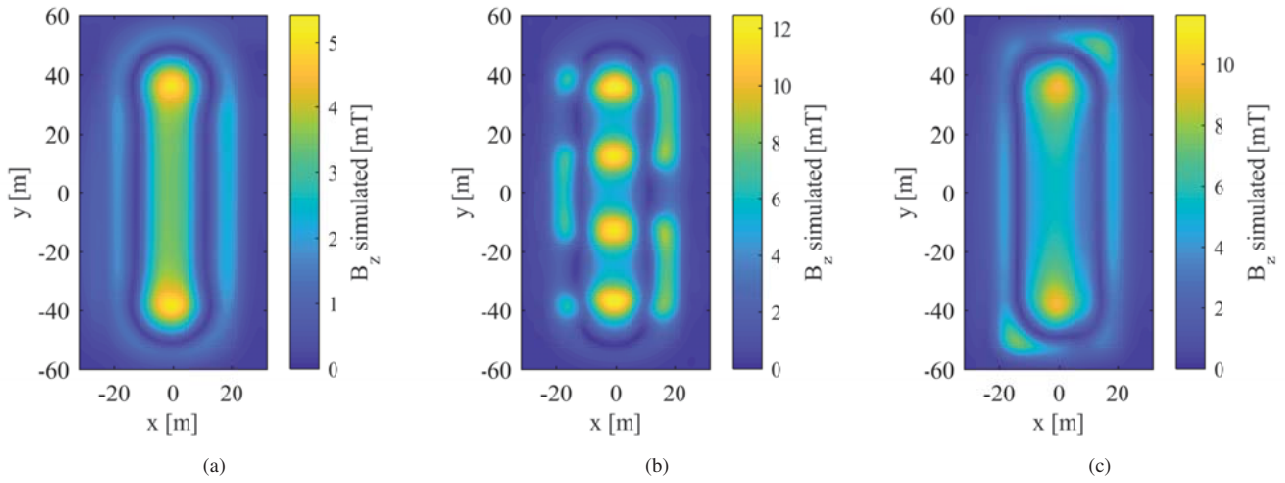

Fig. 6. Simulated magnetic flux density in the z-direction with the developed model. a) Plate 1. b) Plate 2. c) Plate 3.
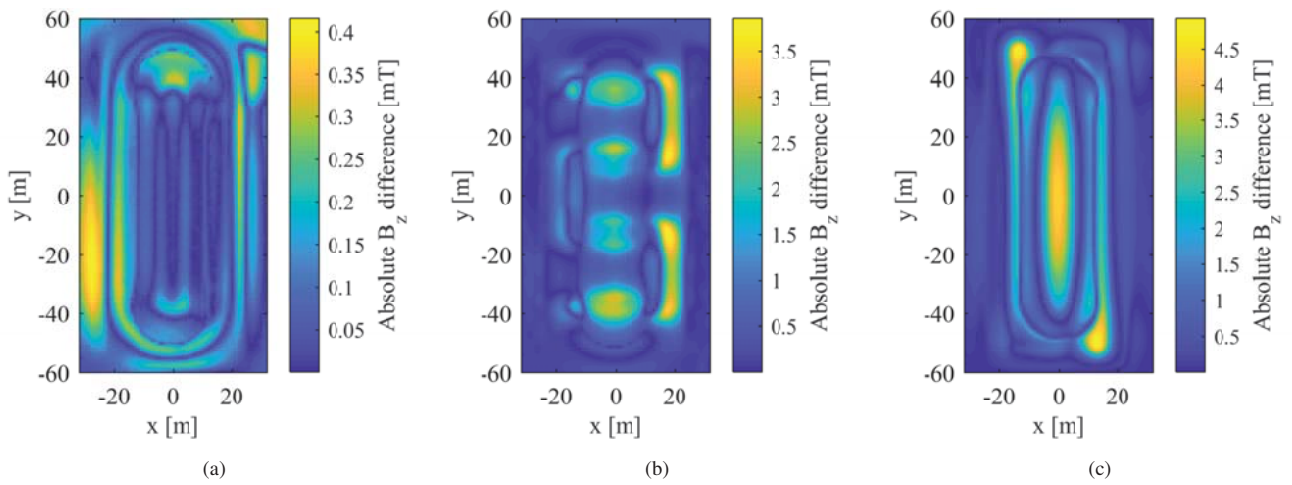

Fig. 7. Absolute difference between the measured and simulated magnetic flux density in the z-direction with the experimental setup. a) Plate 1. b) Plate 2. c) Plate 3.

number of harmonics would enhance the simulated magnetic flux density if a stable and smooth solution can be obtained.

V. CONCLUSION

The paper describes a semi-analytical modeling method, to model eddy currents in slitted conducting plates. The Fourier based solutions include a spatially varying conductivity in the solutions of the magnetic field and induced current density components. The model is compared to measurements on an electromagnetic configuration. The field distribution, due to three different copper plates, of which two contained a slit pattern, placed on a source coil has been analyzed. The modeled magnetic flux density due to the plate without any slits shows a discrepancy of 3 % with the measurement. For the two plates containing slits, the error is around 12 %. This error is caused by measurement uncertainties, such as the exact conductivity value, and by the limitation of the number of harmonics, which needs to be relatively high when the slits have a small width.

REFERENCES

[1] J. W. Jansen, C. M. M. van Lierop, E. A. Lomonova, and A. J. A. Vandenput, "Magnetically levitated planar actuator with moving magnets," in *2007 IEEE International Electric Machines Drives Conference*, vol. 1, May 2007, pp. 272–278.

[2] J. M. M. Rovers, J. W. Jansen, and E. A. Lomonova, "Design and measurements of the double layer planar motor," in *Electric Machines Drives Conference (IEMDC), 2013 IEEE International*, May 2013, pp. 204–211.

[3] L. Zhang, B. Kou, F. Xing, and B. Zhao, "Characteristic analysis of an ironless linear synchronous motor with novel halbach magnet array," in *2014 17th International Symposium on Electromagnetic Launch Technology*, July 2014, pp. 1–5.

[4] J. M. M. Rovers, J. W. Jansen, and E. A. Lomonova, "Disturbance effects of electrically conductive material in the air gap of a linear permanent magnet synchronous motor," *Magnetics, IEEE Transactions on*, vol. 47, no. 10, pp. 2668–2671, Oct 2011.

[5] L. Zhang, B. Kou, Y. Chen, and Y. Jin, "Analysis and calculation of eddy current braking force for an ironless linear synchronous motor with cooling system," in *2016 19th International Conference on Electrical Machines and Systems (ICEMS)*, Nov 2016, pp. 1–5.

[6] C. H. H. M. Custers, T. T. Overboom, J. W. Jansen, and E. A. Lomonova, "2-D semianalytical modeling of eddy currents in segmented structures," *IEEE Transactions on Magnetics*, vol. 51, no. 11, pp. 1–4, Nov 2015.

[7] J. P. C. Smeets, T. T. Overboom, J. W. Jansen, and E. A. Lomonova, "Three-dimensional analytical modeling technique of electromagnetic fields of air-cored coils surrounded by different ferromagnetic boundaries," *Magnetics, IEEE Transactions on*, vol. 49, no. 12, pp. 5698–5708, Dec 2013.